Efficient photoluminescent thin films consisting of anchored hybrid perovskite nanoparticles

Laura Martínez-Sarti,[a] Teck Ming Koh,[b] Maria-Grazia La-Placa,[a] Pablo P. Boix,[b] Michele Sessolo,[a] Subodh G. Mhaisalkar[b,c] and Henk J. Bolink[a]

[a.] *Instituto de Ciencia Molecular (ICMol), Universidad de Valencia, Catedrático José Beltrán, 2, 46980 Paterna, Spain.*
[b.] *Energy Research Institute @ NTU (ERI@N), Research Techno Plaza, X-Frontier Block, Level 5, 50 Nanyang Drive, 637553 Singapore.*
[c.] *School of Materials Science and Engineering, Nanyang Technological University, 50 Nanyang Avenue, 639798 Singapore.*

Methylammonium lead bromide nanoparticles are synthetized with a new ligand (11-aminoundecanoic acid hydrobromide) by a non-template method. Upon dispersion in toluene they show a remarkable photoluminescence quantum yield of 80%. In addition, the bifunctional ligand allows to anchor the nanoparticles on a variety of conducting and semiconducting surfaces, showing bright photoluminescence films with a quantum yield exceeding 50%. This opens a path for the simple and inexpensive preparation of multilayer light-emitting devices.

Recently, organic inorganic (hybrid) lead halide perovskites have been widely studied for photovoltaic applications, where power conversion efficiencies exceeding 22.1% have been demonstrated.[1, 2] Beyond solar cells, these materials are interesting candidates for low-threshold lasers and light-emitting diodes (LEDs).[1, 3-7] Their application in LEDs requires a precise control over their morphology, since this determines their optical and electronic properties.[8, 9] In particular, materials with high photoluminescent quantum yield (PLQY) are desirable for the preparation of efficient LEDs. One of the most suitable strategies for controlling the morphology and enhancing the photoluminescence of perovskites is the preparation of nanostructured materials. In nanostructured perovskites, the spatial confinement of the charge carriers, together with a passivation of the surface states result in a substantial increase of the luminescence yield when compared to bulk perovskites.[10] The recent breakthroughs in the PLQY of narrow-band emitting perovskite nanoparticles (NPs) (full width at half-maximum, FWHM ~20 nm) make these materials promising candidates for light-emitting applications.[11, 12] Perovskite NPs can be prepared by a direct, non-template method that makes use of organic ligands to disperse the material in the form of colloidal NPs.[13] These organic capping ligands are usually medium or long chain alkyl ammonium halides that limit the growth of the material in the three dimensions.

Schmidt et al. reported, for the first time, the synthesis of 6-nm sized methylammonium lead bromide ($MAPbBr_3$) colloidal perovskite NPs using octadecylammonium as the capping ligand.[13] Thin films obtained by spin-coating the NPs dispersion showed intense photoluminescence (PL) with an associated quantum yield of about 20%. Through a modified synthetic conditions, the same group later showed that surface states could be further passivated by insertion of a complementary weak Lewis base, and PLQYs up to 82% in solution were obtained.[14] Recently, color tunable mixed halide perovskite NPs with PLQY in solution up to 93% have been demonstrated.[11] Interestingly, the NPs size was found to be strongly dependent on the synthesis temperature, giving an additional degree of freedom in the material design while, at the same time, underlining the difficulties in achieving reproducible preparation of monodisperse hybrid perovskite NPs. The elimination of polar solvents such as dimethylformamide (DMF) during synthesis has been shown to substantially improve the nucleation and growth of $MAPbBr_3$ NPs.[15] In general, however, the PLQY drops substantially when the nanoparticles are processed into thin films, due to unavoidable aggregation of the material.[10] In spite of such reduction of the PLQY, these films have been recently used to prepare LEDs.[16-19] Encouraging brightness and external quantum efficiencies have been shown, further demonstrating the potential of this type of material in lighting and display applications.

In this work, we describe the preparation of highly photoluminescent $MAPbBr_3$ NPs thin-films, through a temperature-independent synthesis which make use of a bifunctional ligand (11-aminoundecanoic acid hydrobromide, $Br^-NH_3^+$-C_{10}-COOH). This molecule efficiently coordinates the NPs and, at the same time, allows to selectively anchor them onto various electroactive surfaces. This approach was then used to construct multi-layer green emitting LEDs. The 11-aminoundecanoic acid was converted into its ammonium bromide salt ($Br^-NH_3^+$-C_{10}-COOH) to enhance its solubility in DMF. The NPs were obtained taking advantage of the interplay between a polar solvent (DMF, able to solubilize the perovskite precursors) and a non-polar one (toluene), as described in previously published protocols.[11, 13] The perovskite precursors (MABr and $PbBr_2$) were dissolved in DMF (ratio 1:1, 0.04 M), together with oleic acid (to avoid the NPs aggregation) and varying amounts of $Br^-NH_3^+$-C_{10}-COOH. A small volume of this solution was injected into toluene under vigorous stirring. The resulting solution was centrifuged in order to remove larger aggregates, and a bright luminescent supernatant suspension was obtained.

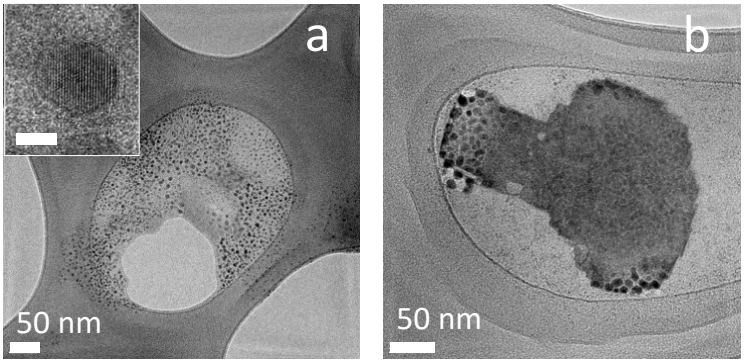

Fig. 1 Absorption (gray) and PL spectra (blue and green) of $MAPbBr_3$ NPs colloidal solutions in toluene for $Br^-NH_3^+$-C_{10}-COOH/MA molar ratio of (a) 2 and (b) 0.5. Insets: photographs of each colloidal solution under UV excitation (λ = 365 nm).

By modifying the ligand amount, a strong variation in the optical properties of the suspension was observed. In particular, when a molar ratio of $Br^-NH_3^+$-C_{10}-COOH/MA = 2 was used during the synthesis, a blue light emitting NPs suspension was obtained (Fig. 1a). This dispersion showed a maximum PL emission at 490 nm, FWHM of 22 nm, and PLQY of 25%. The influence of the long chain ammonium ligand $Br^-NH_3^+$-C_{10}-COOH on the color of the resulting suspension is a result of the equilibrium between the formation of three dimensional $MAPbBr_3$ NPs and two dimensional structures where the ligand itself participate in the formation of layered perovskites.[10, 20-22] In particular, with an excess of $Br^-NH_3^+$-C_{10}-COOH, mainly 2D perovskite nanostructures are obtained. In these materials, the long chain cations alternate inorganic sheets of octahedral lead bromide, resulting in a multi-well, dielectric-semiconductor structure characterized by an increased exciton binding energy.[20] The formation of such structures leads to an intense and sharp peak in the low energy part of the absorption spectra, as is clearly visible in the case of our suspensions prepared with high ligand content (Fig. 1a). On the other hand, by reducing the amount of ligand used to a molar ratio of $Br^-NH_3^+$-C_{10}-COOH/MABr = 0.5, the typical $MAPbBr_3$ absorption and emission spectra can be observed, as a footprint of 3D NPs formation (Fig. 1b). This dispersion showed narrow and intense photoluminescence (centered at 521 nm, with FWHM of about 20 nm) with an associated PLQY as high as 80%. As mentioned before, the temperature of the non-polar solvent (here toluene) was reported to be of special importance, defining the size and hence the emission wavelength of the NPs.[11]

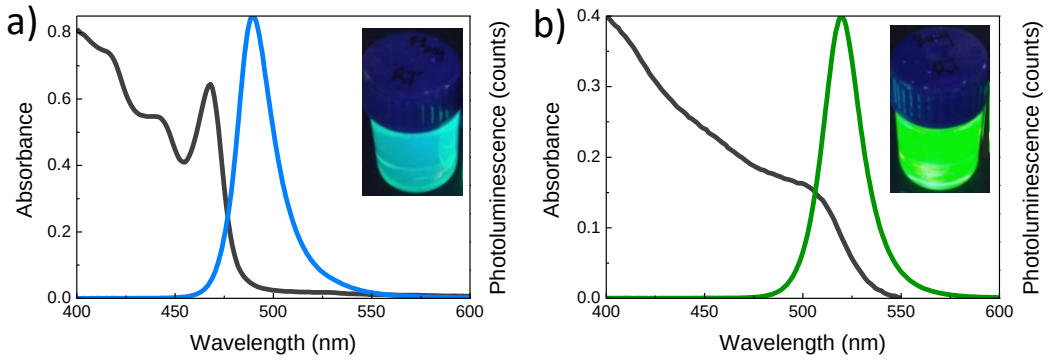

Fig. 2 (a) TEM image of the $MAPbBr_3$ NPs prepared using a molar ratio $Br^-NH_3^+$-C_{10}-COOH/MABr = 0.5 at 25 ºC (Fig. 1a). Inset: High resolution TEM image of an isolated NP (scale bar 4 nm). (b) TEM image of the perovskite nanostructures obtained in the presence of an excess of $Br^-NH_3^+$-C_{10}-COOH at 25 ºC (Fig. 1b).

Interestingly, the synthesis in the presence of $Br^-NH_3^+$-C_{10}-COOH was found to be rather temperature independent. In fact, when the synthesis is carried out at 60 ºC, the absorption and luminescence spectra of the obtained NPs suspension are similar to those prepared at room temperature (Fig. S1, ESI). We investigated the morphology of the NPs suspensions prepared at 25 ºC by transmission electron microscopy (TEM). The electron microscopy confirmed the presence of the perovskite NPs (Fig. 2a) with a diameter in the 3-10 nm range (4.5 nm in average, see Fig. S5 for details). With increased $Br^-NH_3^+$-C_{10}-COOH content, the morphology changes showing wide 2D sheets (50-200 nm) embedding spherical nanocrystals (Fig. 2b). This mixture of nanostructures has been described in several reports, and results from the competition among the formation of 3D and 2D-type perovskites, as described before.[13, 23] The choice of the cationic ligand $Br^-NH_3^+$-C_{10}-COOH was made in order to enable efficient coordination to the perovskite NPs and, thanks to the carboxyl group, allow for the anchoring of the NPs on functional surfaces, such as metal oxides.[24] Moreover, the carboxyl group reduces the QD aggregation enhancing the stability of the NPs suspension, in analogy to the function of the oleic acid additive.[11] Hence, we tested the adhesion of the NPs onto thin films of ZnO, a n-type semiconductor widely used as electron injection layer in OLEDs.[25] 150 nm thick ZnO layers were prepared by spin-coating and high temperature annealing (400 ºC) of a commercial ZnO NPs suspension, on indium tin oxide (ITO) coated glass substrates. These ZnO coated substrates were immersed into the NPs suspension for 12 hours and then rinsed with toluene before characterization. The ZnO/$MAPbBr_3$ NPs films exhibited bright photoluminescence under UV excitation (λ = 365 nm) (Fig. 3a, inset), with a maximum PL emission at 514 nm and FWHM of 25 nm (Fig. 3a). Importantly, the associated PLQY of the thin films was as high as 52% when excited at 380 nm. Despite the decrease of the PLQY from dispersion to the solid state, this value is among the highest reported

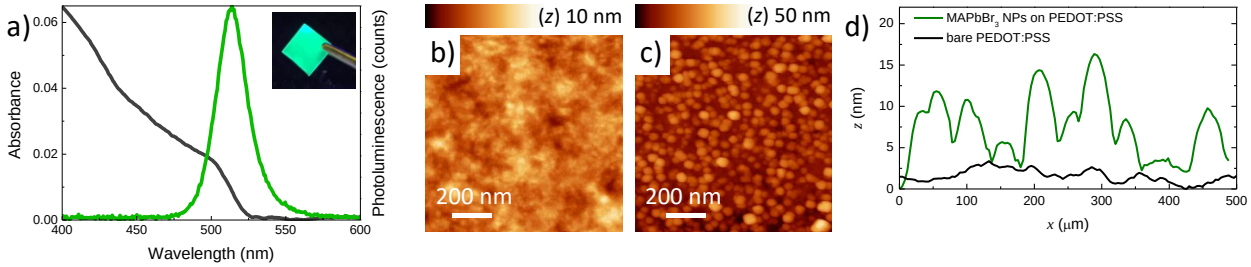

Fig. 3 (a) Absorption (gray) and PL (green) spectra of the $MAPbBr_3$ NPs anchored to a ZnO substrate. Inset: photograph of a ZnO/NPs film under UV excitation (λ = 365 nm). AFM topographies of a PEDOT:PSS film without (b) and with (c) the anchored perovskite NPs. Note the different vertical scale used for the images. (d) Comparison of the surface profile of the same two samples.

for perovskite NPs thin films, most likely thanks to the anchoring of the NPs which strongly inhibit their aggregation. Time-resolved PL measurements were performed both on the colloidal solution and on the ZnO films functionalized with the NPs (Fig. S4). In accordance with previous

reports, the average lifetime for the NPs suspension was found to be 65 ns, with a long tail extending towards the microsecond timescale.[11, 14] On the other hand, the excited state lifetime was found to be substantially reduced (11 ns) when the $MAPbBr_3$ NPs where anchored to the ZnO surface, due to efficient electron transfer from the perovskite to the ZnO valence band.[26] The efficient charge transfer could also partially explain the PLQY reduction observed for the anchored $MAPbBr_3$ NPs. Importantly, the ZnO/$MAPbBr_3$ NPs films maintained their luminescence after washing with toluene, implying that the NPs were effectively anchored to the surface. This is very important since other functional layers (i.e. organic charge transport materials) can be coated on top of the perovskite NPs, allowing for the preparation of multilayer LEDs.

In order to investigate the morphology of the NPs anchored on the ZnO NPs film, atomic force microscopy (AFM) was used. The rather rough ZnO surface (Fig. S2, ESI), however, made it difficult to discern the perovskite NPs. Hence, we looked for a substantially more flat surface compared to the solution processed ZnO that would allow a direct visualization of the perovskite NPs. We selected poly(3,4-ethylenedioxythiophene) doped with poly(styrene sulphonate) (PEDOT:PSS) as a test platform to anchor the $MAPbBr_3$ NPs. In spite of the very different chemical nature of PEDOT:PSS compared to ZnO, the perovskite NPs did also adhere on the conducting polymer coated substrate, and the films exhibited a maximum PL emission at 513 nm and a PLQY of 50%, analogous to what was observed for the ZnO/NPs systems (Fig. S3, ESI).

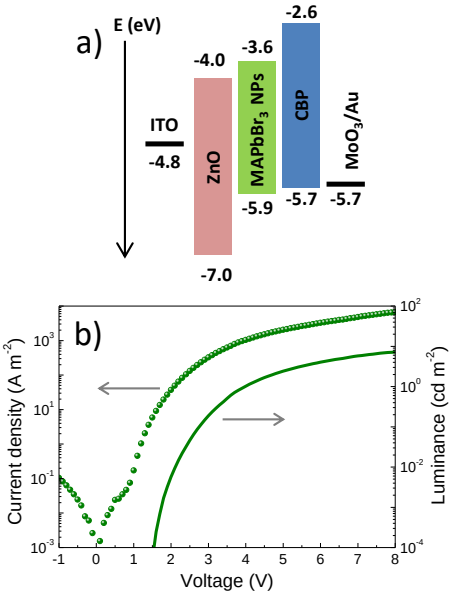

Fig. 4 (a) Flat band energy diagrams of the materials used in the NPs LEDs. (b) Current density (symbols) and luminance (line) versus applied bias for the same device.

The adhesion of the perovskite NPs on PEDOT:PSS is most likely promoted by the large amount of ionic groups present in the conducting polymer, leading to a favorable electrostatic interaction between the carboxyl groups of the ligands and the surface. The morphology of the PEDOT:PSS/NPs thin films were analyzed by AFM. The surface of the PEDOT:PSS film is flat and homogeneous (Fig. 3b), with an associated root-mean-square roughness of only 1.2 nm, calculated over a 2 x 2 μm area. The same surface, when coated with the perovskite NPs, is composed by densely packed particles (Fig. 3c), whose dimensionality can be estimated by measuring the surface profile (Fig. 3d). Structures with height varying from about 5 to 15 nm can be observed, indicating a low roughness and hence limited aggregation of the NPs on the surface (considering the particle size distribution obtained from TEM analysis). The lateral size of the particles, as observed from the AFM profiles, appears much larger as it is a deconvolution of the surface and the AFM tip. From this morphological analysis and considering the unchanged optical properties of the NPs when anchored to ZnO or PEDOT:PSS, we conclude that the $MAPbBr_3$ NPs are grafted on the semiconducting ZnO surface, where they form homogeneous and compact films, suitable for the fabrication of optoelectronic devices. Hence, multilayer LEDs with n-i-p configuration (n-type layer deposited on the transparent substrate) were prepared. The ZnO

sensitized with $MAPbBr_3$ NPs was deposited on ITO coated glass substrates, and a 100 nm thick CBP film (4,4′-Bis(N-carbazolyl)-1,1′-biphenyl, acting as the hole transport layer, HTL) was spin-coated on top from its chlorobenzene solution (20 mg mL^{-1}). The device was finished by vacuum deposition of a thin (10 nm) layer of MoO_3 (facilitating hole injection from the anode to the CBP) and a 100 nm thick gold anode on top. The flat band energy diagram for the materials used in the device is depicted in Fig. 4a.

The current density and luminance versus voltage characteristics for a device using $MAPbBr_3$ NPs as the emitting material is reported in Fig. 4b. The current density to voltage behavior shows a typical diode characteristic (low leakage, exponential forward current injection), highlighting the good quality of the device and layers used. The LED turns on at about 1.5 V applied bias, reaching a luminance of 8 cd m^{-2} at 8 V. Unfortunately, the current density at the same applied bias is very high ($8 \cdot 10^3$ A m^{-2}), limiting the overall current efficiency to about 10^{-3} cd A^{-1}. This can be a consequence of the extremely thin perovskite NPs layer used (virtually a monolayer), limiting the attainable electroluminescence. An uneven particle distribution causing insufficient coverage could also reduce the overall current efficiency. On the other hand, the ZnO layer used is not completely flat and can hence cause an uneven distribution of the applied field or direct electron-hole recombination at the ZnO surface. It is known that the nanocrystalline morphology of the oxide film plays an important role in determining the electroluminescence process.[27] Considering that indeed LEDs employing a monolayer of luminescent NPs have been demonstrated,[28] a more homogeneous and especially flat surface would be desirable when using $MAPbBr_3$ NPs. Unfortunately, inverted device (p-i-n) employing PEDOT:PSS/$MAPbBr_3$ NPs in combination with an electron transport layer showed no electroluminescence at all. This is not surprising since the PEDOT:PSS/$MAPbBr_3$ is not a blocking interface, and direct charge recombination at the conducting polymer is favored.

In summary, a temperature-independent synthesis of $MAPbBr_3$ nanoparticles (NPs) employing the ammonium salt of 11-aminoundecanoic acid ($Br^-NH_3^+$-C_{10}-COOH) as ligand has been developed. Dispersions of NPs with a diameter below 10 nm and a PLQY of about 80% can be readily obtained at room-temperature and in atmospheric conditions. Thanks to the use of the $Br^-NH_3^+$-C_{10}-COOH bifunctional ligand, the NPs can be anchored on a variety of electroactive surfaces, such as inorganic semiconductors or conducting polymers. The NPs anchored to ZnO and PEDOT:PSS thin films showed remarkable photoluminescence quantum yield of approximately 50%. The NPs-sensitized ZnO films can be directly integrated into light-emitting devices, leading to modest but homogeneous light-emission. The anchoring of perovskite NPs on several flat and semiconducting surfaces is being investigated, with the potential of opening new paths for the preparation of simple and inexpensive multilayer light-emitting devices.

We acknowledge financial support from the European Union H2020 project INFORM (grant 675867), the Spanish Ministry of Economy and Competitiveness (MINECO) via the Unidad de Excelencia María de Maeztu MDM-2015-0538, MAT2014-55200 and PCIN-2015-255 and the Generalitat Valenciana (Prometeo/2012/053). M.S. thanks the MINECO for a post-doctoral (JdC) contract. T.M. Koh, P.P. Boix and S.G. Mhaisalkar would like to acknowledge the funding from Singapore NRF through the Competitive Research Program: NRF-CRP14-2014-03 as well as from NTU-A*STAR Silicon Technologies Centre of Excellence under the program grant no. 112 3510 0003.

References

1. S. D. Stranks and H. J. Snaith, *Nature Nanotechnology*, 2015, **10**, 391-402.
2. Q. Wang, H. Chen, G. Liu and L. Wang, *Science Bulletin*, 2015, **60**, 405-418.
3. G. Xing, N. Mathews, S. S. Lim, N. Yantara, X. Liu, D. Sabba, M. Grätzel, S. Mhaisalkar and T. C. Sum, *Nature Materials*, 2014, **13**, 476-480.
4. N. Yantara, S. Bhaumik, F. Yan, D. Sabba, H. A. Dewi, N. Mathews, P. P. Boix, H. V. Demir and S. Mhaisalkar, *The Journal of Physical Chemistry Letters*, 2015, **6**, 4360-4364.
5. B. R. Sutherland and E. H. Sargent, *Nature Photonics*, 2016, **10**, 295-302.

6. P. Docampo and T. Bein, *Accounts of Chemical Research*, 2016, **49**, 339-346.
7. S. A. Veldhuis, P. P. Boix, N. Yantara, M. Li, T. C. Sum, N. Mathews and S. G. Mhaisalkar, *Advanced Materials*, 2016, DOI: 10.1002/adma.201600669, n/a-n/a.
8. N. K. Kumawat, A. Dey, K. L. Narasimhan and D. Kabra, *ACS Photonics*, 2015, **2**, 349-354.
9. J. C. Yu, D. B. Kim, E. D. Jung, B. R. Lee and M. H. Song, *Nanoscale*, 2016, **8**, 7036-7042.
10. S. González-Carrero, R. E. Galian and J. Pérez-Prieto, *Particle & Particle Systems Characterization*, 2015, **32**, 709-720.
11. H. Huang, A. S. Susha, S. V. Kershaw, T. F. Hung and A. L. Rogach, *Advanced Science*, 2015, **2**, n/a-n/a.
12. L. Protesescu, S. Yakunin, M. I. Bodnarchuk, F. Krieg, R. Caputo, C. H. Hendon, R. X. Yang, A. Walsh and M. V. Kovalenko, *Nano Letters*, 2015, **15**, 3692-3696.
13. L. C. Schmidt, A. Pertegás, S. González-Carrero, O. Malinkiewicz, S. Agouram, G. Mínguez Espallargas, H. J. Bolink, R. E. Galian and J. Pérez-Prieto, *Journal of the American Chemical Society*, 2014, **136**, 850-853.
14. S. Gonzalez-Carrero, R. E. Galian and J. Pérez-Prieto, *J. Mater. Chem. A*, 2015, **3**, 9187-9193.
15. O. Vybornyi, S. Yakunin and M. V. Kovalenko, *Nanoscale*, 2016, **8**, 6278-6283.
16. M. F. Aygüler, M. D. Weber, B. M. D. Puscher, D. D. Medina, P. Docampo and R. D. Costa, *The Journal of Physical Chemistry C*, 2015, **119**, 12047-12054.
17. H. Huang, F. Zhao, L. Liu, F. Zhang, X.-g. Wu, L. Shi, B. Zou, Q. Pei and H. Zhong, *ACS Applied Materials & Interfaces*, 2015, **7**, 28128-28133.
18. W. Deng, X. Xu, X. Zhang, Y. Zhang, X. Jin, L. Wang, S. T. Lee and J. Jie, *Advanced Functional Materials*, 2016, DOI: 10.1002/adfm.201601054.
19. Y. Ling, Z. Yuan, Y. Tian, X. Wang, J. C. Wang, Y. Xin, K. Hanson, B. Ma and H. Gao, *Advanced Materials*, 2016, **28**, 305-311.
20. D. B. Mitzi, K. Chondroudis and C. R. Kagan, *IBM Journal of Research and Development*, 2001, **45**, 29-45.
21. D. Sapori, M. Kepenekian, L. Pedesseau, C. Katan and J. Even, *Nanoscale*, 2016, **8**, 6369-6378.
22. S. Bhaumik, S. A. Veldhuis, Y. F. Ng, M. Li, S. K. Muduli, T. C. Sum, B. Damodaran, S. Mhaisalkar and N. Mathews, *Chemical Communications*, 2016, **52**, 7118-7121.
23. P. Tyagi, S. M. Arveson and W. A. Tisdale, *The Journal of Physical Chemistry Letters*, 2015, **6**, 1911-1916.
24. E. Galoppini, *Coordination Chemistry Reviews*, 2004, **248**, 1283-1297.
25. M. Sessolo and H. J. Bolink, *Advanced Materials*, 2011, **23**, 1829-1845.
26. H. B. Kim, I. Im, Y. Yoon, S. D. Sung, E. Kim, J. Kim and W. I. Lee, *Journal of Materials Chemistry A*, 2015, **3**, 9264-9270.
27. Y. Athanassov, F. P. Rotzinger, P. Péchy and M. Grätzel, *The Journal of Physical Chemistry B*, 1997, **101**, 2558-2563.
28. S. Coe, W.-K. Woo, M. Bawendi and V. Bulovic, *Nature*, 2002, **420**, 800-803.

Supporting Information

Efficient photoluminescent thin films consisting of anchored hybrid perovskite nanoparticles

Laura Martínez-Sarti, Teck Ming Koh, Maria-Grazia La-Placa, Pablo P. Boix, Michele Sessolo, Subodh G. Mhaisalkar and Henk J. Bolink

[a] Instituto de Ciencia Molecular (ICMol), Universidad de Valencia, Catedrático José Beltrán, 2, 46980 Paterna, Spain.
[b] Energy Research Institute @ NTU (ERI@N), Research Techno Plaza, X-Frontier Block, Level 5, 50 Nanyang Drive, 637553 Singapore.
[c] School of Materials Science and Engineering, Nanyang Technological University, 50 Nanyang Avenue, 639798 Singapore.

Synthesis of the $MAPbBr_3$ NPs and sensitized ZnO films

For the $MAPbBr_3$ NPs fabrication, the 11-aminoundecanoic acid was initially converted into its ammonium salt with an excess of HBr, to enhance its solubility in DMF. $PbBr_2$ (0.04 M) and 474 µL of oleic acid were dissolved in 2.5 mL of DMF (solution A). Subsequently, 596 µL of this solution were added into 0.5 mL of another DMF solution B containing MABr (0.04 M) and varying amounts of $Br^-NH_3^+$-C_{10}-COOH. 0.5 mL of this precursor solution (A+B) was quickly injected into toluene (5 mL) under vigorous stirring at room temperature (RT) or previously heated at 60 ºC. A yellow-green solution was immediately observed, consequence of the formation of the NPs. The solution was centrifuged at 12.5 krpm for 10 minutes to remove larger aggregates, and a bright luminescent supernatant solution was obtained.

For coating the ZnO films, 0.5 mL of a solution of 40 wt% in ethanol from Sigma-Aldrich (average particle size of 35 nm) were diluted in 3 mL of ethanol, and then spin-coated using a GYRSET® (closed cover coating technology). The layers were then annealed at 450 ºC during 30 min.

For the ZnO/$MAPbBr_3$ NPs films preparation, the ZnO coated substrates were immersed into the NPs suspension for 12 hours and subsequently rinsed with toluene.

Characterization

The photoluminescence (PL) characteristics were studied using a Xe lamp coupled to a monochromator as the excitation source and an integrated sphere coupled to a spectrometer (Hamamatsu C9920-02 with a Hamamatsu PMA-11 optical detector) in order to quantitatively determine the PLQY. UV-visible absorption spectra of the films were collected using a fiber-optics based Avantes Avaspec2048 spectrophotometer. UV-visible spectra of the dispersions were recorded using a quartz cuvettes spectrometer in a UV-visible spectrophotometer Agilent 8453E. TEM and high resolution TEM (HR-TEM) were performed with a Field Emission Gun (FEG) TECNAI G2 F20 microscope operated at 200 kV. LEDs were characterized under inert conditions inside a glovebox. The current density and luminance versus voltage characteristics were measured using a Keithley 2400 Source-Meter and a photodiode coupled to a Keithley 6485 pico-ammeter, using a Minolta LS100 camera to calibrate the photocurrent. The AFM images were collected with a Digital Instrument Veeco Nanoscope IVa AFM microscope in tapping mode, using silicon tips with natural resonance frequency of 320 kHz and with an equivalent constant force of 42 N m^{-1}.

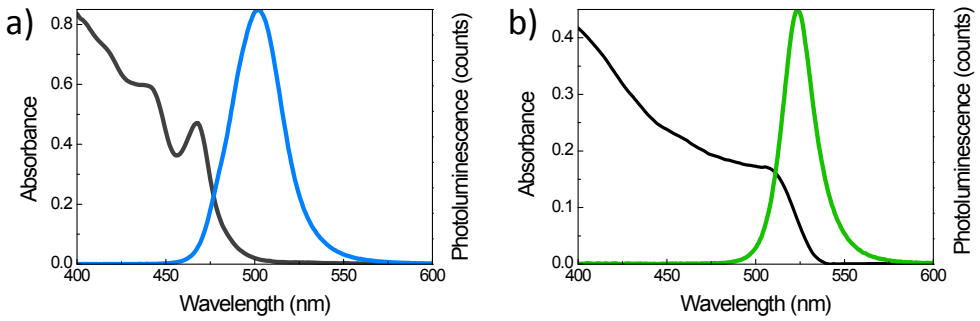

Fig. S1 Absorption (gray) and PL spectra (blue and green) of $MAPbBr_3$ NPs colloidal solutions in toluene at 60 ºC for $Br^-NH_3^+$-C_{10}-COOH/MA molar ratio of (a) 2 and (b) 0.5.

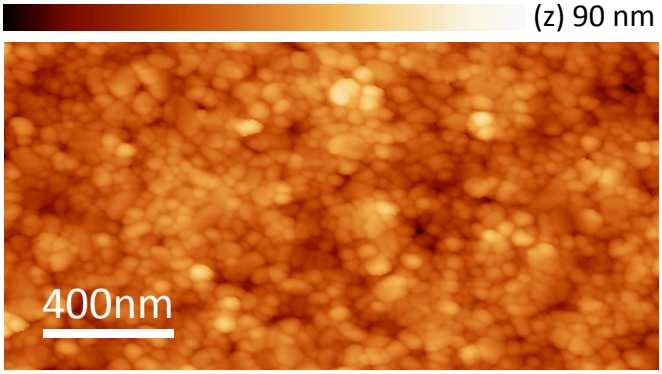

Fig. S2 AFM topography of a solution-processed ZnO film.

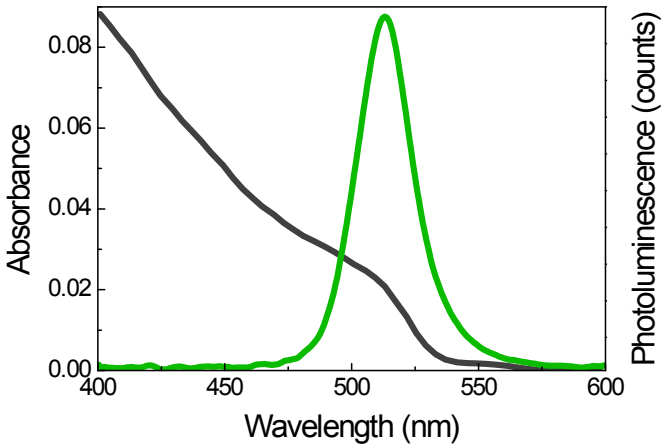

Fig. S3 Absorbance (gray) and photoluminescence (green) spectra of the $MAPbBr_3$ NPs anchored to a PEDOT:PSS substrate.

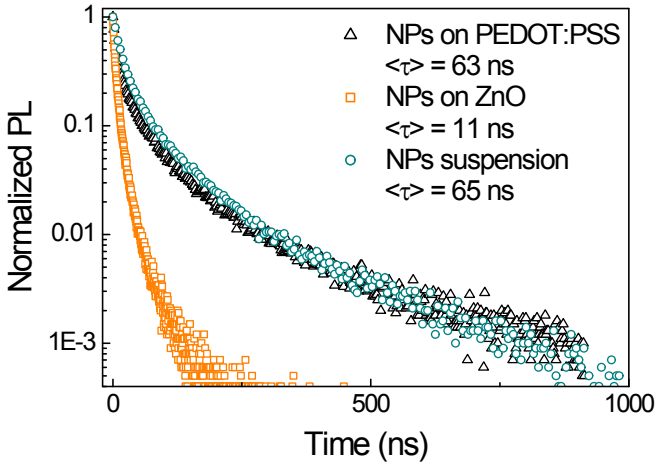

Fig. S4 Time-resolved PL measurements taken at the peak emission wavelength (521 nm) of the $MAPbBr_3$ NPs colloidal solution and the NPs anchored on ZnO and PEDOT:PSS thin films, with a pump wavelength of 405 nm.

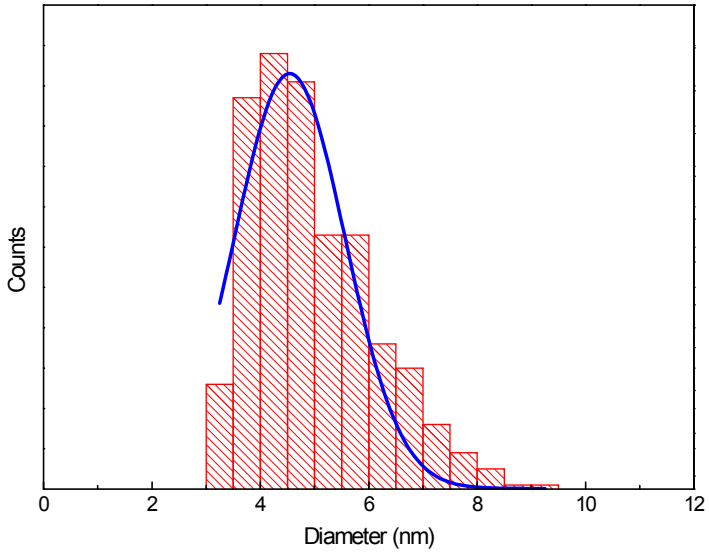

Fig. S5 Particle size histograms calculated from the TEM image in Fig. 2a, plotted from analysis of >500 particles. Mean and standard deviation for the distribution are 4.6 and 2.4 nm, respectively.